Metastable cubic tin sulfide: A novel phonon-stable chiral semiconductor

Jonathan M. Skelton, Lee A. Burton, Fumiyasu Oba, and Aron Walsh

Citation: APL Materials **5**, 036101 (2017); doi: 10.1063/1.4977868
View online: http://dx.doi.org/10.1063/1.4977868
View Table of Contents: http://aip.scitation.org/toc/apm/5/3
Published by the American Institute of Physics

Metastable cubic tin sulfide: A novel phonon-stable chiral semiconductor

Jonathan M. Skelton,[1] Lee A. Burton,[2] Fumiyasu Oba,[2] and Aron Walsh[3,4]
[1]*Centre for Sustainable Chemical Technologies and Department of Chemistry, University of Bath, Claverton Down, Bath BA2 7AY, United Kingdom*
[2]*Laboratory for Materials and Structures, Institute of Innovative Research, Tokyo Institute of Technology, 4259 Nagatsuta, Midori-ku, Yokohama 226-8503, Japan*
[3]*Department of Materials Science and Engineering, Yonsei University, Seoul, South Korea*
[4]*Department of Materials, Imperial College London, Exhibition Road, London SW7 2AZ, United Kingdom*

(Received 14 January 2017; accepted 20 February 2017; published online 7 March 2017)

SnS is a semiconductor of interest for next-generation thin-film photovoltaic devices. The ground-state phase is layered with an orthorhombic (*Pnma*) crystal structure. Anisotropy in the electrical properties has been linked to the low performance of SnS solar cells. These factors make a new cubic phase (π-SnS) of immense practical interest. We report the properties of the recently solved crystal structure ($P2_13$) of cubic SnS from first-principles. π-SnS is phonon stable, in contrast to the zincblende phase, and lies 2.2 kJ/mol above the ground state. It features an electronic bandgap of 1.7 eV with a chiral modulation of the band-edge states.
[http://dx.doi.org/10.1063/1.4977868]

Tin monosulfide (SnS) has been studied as a semiconductor since the 1960s,[1] with the first report of an SnS photovoltaic cell in 1994 having an efficiency of 0.3%.[2] With over 20 years of research effort, the performance of the champion SnS solar cell still falls below 5% light-to-electricity conversion.[3,4]

SnS is naturally found as the mineral herzenbergite, with a characteristic orthorhombic crystal structure (*Pnma* type) consisting of bi-layers of SnS stacked along the *c* axis forming a natural (001) cleavage plane. It is known that the physical properties of SnS are anistropic,[5] e.g., the effective masses of holes are five times larger along <001> than <100> and <010>.[1] In addition, the work functions of the crystal vary significantly for different crystal terminations.[6,7] There is a consensus in the thin-film photovoltaic community that this anisotropy is a source of performance loss due to inefficient collection of photogenerated charge carriers in solar cells.[7]

There have been long-standing reports of "cubic" SnS.[8] A rocksalt-structured phase ($Fm\bar{3}m$ type) of SnS is accessible under external pressure or epitaxial strain;[9] however, the more recent reports concern thin-films stable under ambient conditions.[10–12] To date, this cubic phase has been synthesised using a variety of deposition techniques including aerosol-assisted chemical-vapour deposition (CVD),[13] chemical-bath deposition,[11] and successive ionic-layer adsorption and reaction.[12]

The widespread assignment of a zincblende ($F\bar{4}3m$ type) crystal structure to the cubic phase was challenged on the basis of first-principles density-functional theory (DFT) calculations, which demonstrated that this phase was both high in energy and not dynamically stable in finite-temperature molecular-dynamics simulations.[14] It was suggested that the observed cubic phase was, instead, related to the rocksalt structure. Nonetheless, assignment of a zincblende phase of SnS continued in the literature,[13] until, recently, a new cubic crystal structure was resolved, using electron and X-ray diffraction, corresponding to a 2×2×2 supercell expansion of the rocksalt structure with large internal distortions.[15] The phase has been named π-SnS (see Figure 1).

In this letter, we assess the physical properties of π-SnS from first-principles theory. We confirm that π-SnS is phonon stable across the vibrational Brillouin zone. The new phase is close in energy to the ground-state orthorhombic phase, and significantly lower in energy than the zincblende phase. We further show that the chiral space group adopted by π-SnS results in an unusual electronic band

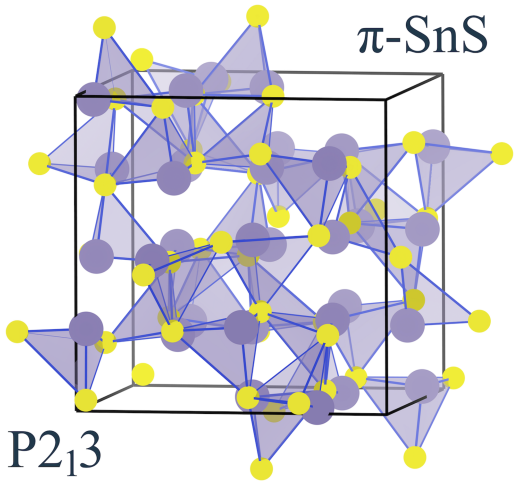

FIG. 1. Illustration of the crystallographic unit cell of the new metastable cubic phase of SnS. There are 32 formula units in the cell with a = 11.5 Å. The Sn-centred polyhedra are shaded grey, with sulfur atoms colored yellow.

structure with modulations of the band extrema away from the high-symmetry points. An electronic bandgap of 1.74 eV is calculated, with a large high-frequency dielectric constant of 11.5. This novel material offers attractive properties for applications in solar-energy conversion and non-linear optics. The theoretical Shockley–Queisser limit remains above 25% and the larger bandgap could be beneficial for high voltage applications including solar fuel generation.

Concerning the crystal structure of π-SnS, in 2015 Golan and coworkers initially assigned the $P2_13$ space group with a lattice constant of 11.7 Å and a 64-atom unit cell based on electron-diffraction experiments.[8] This structure is derived from rocksalt rather than zincblende, and is consistent with nanoparticles of a tetrahedral morphology.[16] The assignment was further supported by X-ray diffraction data.[15] The cubic phase has reported optical bandgaps ranging from 1.6 to 1.8 eV,[11,13,17] and has been used to make a working solar cell.[18]

Starting from the reported crystal structure parameters, we performed a local optimization of the structure (lattice vectors and internal positions) within density-functional theory (DFT) following a quasi-Newton minimization procedure. The equilibrium (DFT/PBEsol) lattice constant of 11.506 Å compares well to the value determined from X-ray diffraction at room temperature (11.603 Å).[15]

Despite the cubic space group, the internal structure of π-SnS appears highly distorted. This originates from the stereochemical activity of the Sn(II) $5s^2$ lone electron pair. Hybridization of the occupied Sn $5s^2$ orbitals with nominally empty $5p^0$ orbitals lowers the energy of the system, but is symmetry-forbidden in an octahedral coordination environment (e.g. for the Sn ions in the rocksalt phase).[19] This second-order Jahn-Teller distortion results in the unusual coordination preferences of the Sn(II) ion. There is an anion dependence of the stereochemical activity, which results in SnO forming a layered structure, SnTe a rocksalt structure, while SnS and SnSe adopt structures with intermediate distortions.[19,20] In π-SnS, each Sn sits in a trigonal pyramidal environment with three short Sn-S bonds (2.7 Å) at the trigonal base and a lone pair projected towards the apex. The polyhedra are connected to form an irregular corner-sharing network.

To assess the dynamic stability of the crystal structure optimized within the $P2_13$ space group, we have computed the harmonic phonon frequencies of the crystal (Figure 2). The phonon dispersion is dense owing to the large number of atoms in the unit cell but all modes have positive frequencies, indicating a local potential-energy minimum. For comparison, we also plot the phonon dispersion of the hypothetical zincblende phase, which shows large instabilities across the Brillouin zone that correspond to a significant fraction of the phonon density of states. We therefore conclude that π-SnS is dynamically stable, while zincblende-SnS is not. Recent Raman measurements of π-SnS found active vibrational modes from 59 to 229 cm^{-1} with a phonon bandgap between 120 and 150 cm^{-1}, in agreement with our predictions.

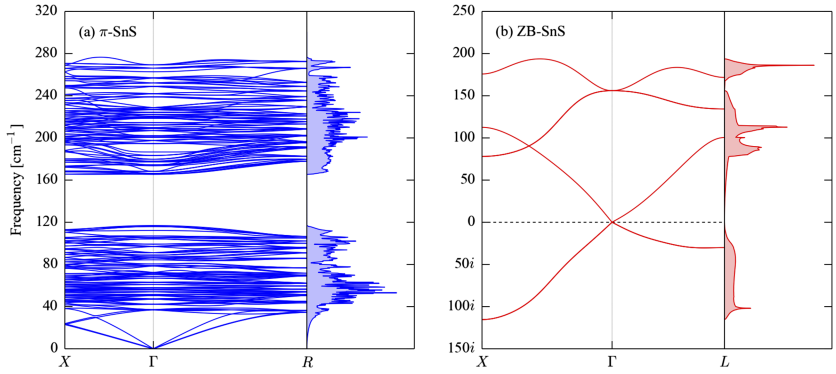

FIG. 2. Harmonic phonon dispersion of (a) π-SnS and (b) zincblende SnS through high-symmetry paths in the respective Brillouin zones. The frequencies were computed from *ab initio* lattice-dynamics calculations using the PBEsol functional (Ref. 21) for electron exchange and correlation. There are 64 atoms in the primitive cell of π-SnS, leading to 192 phonon modes. On each plot, the phonon density of states is shown to the right-hand side of the dispersion.

While these calculations confirm that the cubic phase of SnS is a local minimum in potential energy, we cannot comment on the barrier to transformation to the ground-state orthorhombic phase. The cubic and orthorhombic structures are not connected by crystallographic sub-group relations and the unit cells are not commensurate, so we cannot map a simple pathway between them. Empirically, the cubic phase has been observed to be kinetically stable above the typical operating temperature of a solar cell. No conversion is observed at room temperature, while at 375 °C thin films have been reported to show a phase transition from cubic to orthorhombic over a period of 5 h under N_2.[13]

As an additional test, we compare the total energy of π-SnS to the other phases of this system, which have previously been computed.[14] The new phase is 2.19 kJ/mol above the orthorhombic ground state and 70 kJ/mol below the zincblende phase. This confirms the thermodynamic metastablity of π-SnS and reaffirms the unstable nature of the zinc-blende phase.

Given the confidence in the crystal structure of π-SnS, we can now proceed to the analysis of the electronic structure. The electronic band structure and density of states around the upper valence and lower conduction bands are plotted in Figure 3. The formal electronic configuration of Sn [$5s^2 5p^0$] and S [$3p^6$] is useful conceptually; however, the heteropolar bonding is nuanced. The upper valence

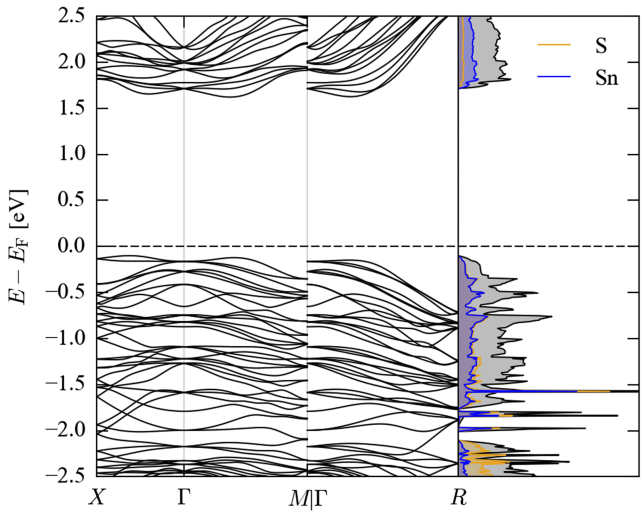

FIG. 3. Electronic band structure (left panel) and ion-projected density of states (right panel) for π-SnS calculated within generalized Kohn-Sham density-functional theory using the hybrid HSE06 functional (Refs. 24 and 25) to model electron exchange and correlation. The minimum direct energy gap is 1.74 eV along the Γ to M line. The high-symmetry labels are taken from the Bilbao crystallographic server.[26]

band (−1.5 to 0 eV with respect to the Fermi level) is a mixture of s and p orbitals from both ions, following the revised lone pair model.[22] The lower conduction band is formed predominately of Sn 5p orbitals. Unusually, the band extrema do not lie at high symmetry points, but rather fall between the Brillouin zone center and the zone boundaries. This feature is common to chiral crystals.[23] Space group $P2_13$ (no. 198) has a point group symmetry T with only rotation and screw symmetry axes, which means that π-SnS may exhibit optical dichroism and a non-linear optical response.

The resulting band edge features are similar to the Rashba/Dresselhaus splitting found in hybrid-halide perovskites;[27] however, this effect is not due to spin-orbit coupling. The minimum direct bandgap of 1.74 eV along Γ to M is slightly larger than the indirect bandgap of 1.72 eV (with a valence-band minimum along Γ to X and a conduction-band minimum along Γ to M), although by a very small margin. The energy difference is small enough that the effect of temperature, through thermal expansion and electron-phonon coupling, could change the nature of the bandgap.

A key descriptor for photovoltaic performance is the dielectric function, as it determines both the frequency-dependent optical absorption profile and the screening between photogenerated charge carriers and charged lattice defects. The computed optical dielectric function is shown in Figure 4. The steep rise in the imaginary dielectric function at the bandgap energy indicates strong optical absorption and is promising for achieving large photocurrents from this material. In contrast, the onset for the orthorhombic phase is less pronounced.[5]

The high-frequency optical dielectric constant is calculated to be 11.5, which is remarkably high in comparison to other materials used in thin film solar cells, e.g., 7 for CdTe[28] and 5 for $CH_3NH_3PbI_3$.[27] Note that using the level of theory employed, quantitative agreement is expected with comparable experimental measurements (usually within 20%). The value is consistent with that of the orthorhombic phase of SnS, where the dielectric constant varies from 11.9 to 12.7 at the same level of theory,[5] in good agreement with measurements from spectroscopic ellipsometry.

In summary, we have demonstrated that π-SnS is a viable alternative to orthorhombic SnS for photovoltaic applications, and may provide a route to overcome the longstanding efficiency bottleneck. The phase is a local potential-energy minimum and is thus dynamically stable. As it is not the thermodynamic global minimum, π-SnS is an example of a metastable semiconductor. We have shown that the phase features a strong optical absorption onset and a large dielectric constant, making it promising for applications in solar energy conversion.

Many interesting questions remain for future exploration. One is the lifetime of the cubic phase, which will be linked to the barrier for transformation to the lower-energy orthorhombic phase. It is not yet clear if a high-quality material suitable for optoelectronic applications can be obtained in the absence of a high temperature annealing process. The surface chemistry and morphology dependence of the physical properties of this new phase are currently unknown. The stability with respect to external stimuli including temperature, pressure, and electric fields is also of interest, especially in

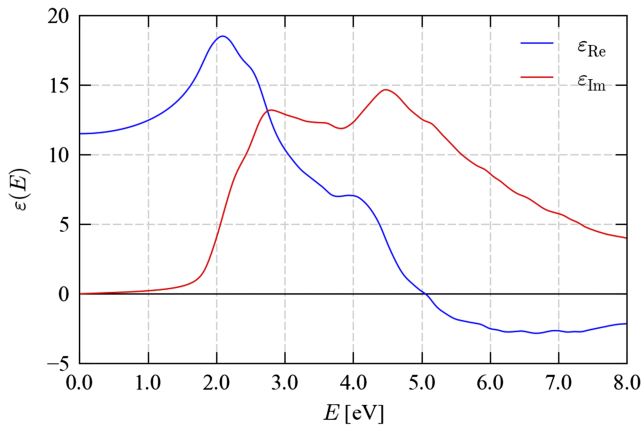

FIG. 4. Real and imaginary dielectric functions for π-SnS calculated within the independent-particle approximation, based on single-particle electronic eigenvalues from the hybrid HSE06 model for electron exchange and correlation (Refs. 24 and 25). Excitonic effects are not included. The value of the high frequency dielectric constant (limit of ε_{Re} at 0 eV) is 11.5.

the context of potential thermoelectric applications.[29,30] The p-type semiconducting behavior of SnS, originating from tin vacancies,[31,32] is expected to be largely unchanged in the cubic phase; however, an explicit investigation of the defect chemistry and physics would certainly be worthwhile.

Computational Methods: First-principles total-energy and force calculations were carried within Kohn-Sham DFT using the VASP code.[33,34] An initial model of the crystal structure was prepared using the data in Ref. 15, and the atomic positions and cell volume optimized to a force tolerance of 10^{-2} eV Å^{-1}. Projector-augmented wave[35] (PAW) core potentials treating the S 3s and 3p and the Sn 5s, 4d, and 5p electrons as valence were used with the PBEsol exchange-correlation functional[21] and a plane-wave cutoff of 550 eV. The Brillouin zone was sampled with a Γ-centred Monkhorst-Pack k-point mesh with 2×2×2 subdivisions. The PAW projection was performed in reciprocal space, and the precision of the charge-density grids was automatically chosen to avoid aliasing errors.

Phonon calculations were carried out using the Phonopy code[36,37] based on forces calculated within DFT as detailed above. A set of force-constant matrices was computed by performing symmetry-inequivalent finite displacements of atoms in a $2 \times 2 \times 2$ expansion of the cubic cell (512 atoms). The k-point sampling was appropriately reduced for these calculations, and an additional support grid with 8× the number of points as the default was used when evaluating the forces. A phonon dispersion and density of states (DoS) curve was obtained using Fourier interpolation. To generate the DoS, phonon frequencies were computed using a regular Γ-centered q-point grid with 48×48×48 subdivisions and interpolated with the linear tetrahedron method.

More accurate electronic-structure calculations were carried out on the optimised structure, using the HSE06 hybrid functional[24,25] in conjunction with a finer $3 \times 3 \times 3$ k-point mesh and 640 electronic bands. A band dispersion was computed using WANNIER90,[38,39] by projecting the 160 highest-lying valence and 160 lowest-energy conduction states onto randomly centered s functions and minimising the quadratic spread to $< 10^{-2}$ A^2. The frequency-dependent dielectric function was calculated using the linear-optics routines in VASP,[40] with the large number of conduction bands (320) ensuring convergence of the sum over unoccupied states.

This research has been supported by the Royal Society, European Research Council (Grant No. 277757) and the EPSRC (EP/J017361/1, EP/K004956/1, EP/K016288/1, EP/L017792/1, EP/M009580/1, EP/G03768X/1). This work benefitted from access to the SiSu supercomputer at the CSC - IT Center for Science, Finland, via the Partnership for Advanced Computing in Europe (PRACE) initiative (Project no. 13DECI0317, IsoSwitch). Calculations were also performed on the Balena HPC cluster at the University of Bath, which is maintained by the Bath University Computing Services. L.A.B. is an International Research Fellow of the Japan Society of Promotion of Science (JSPS; Grant No. 26.04792).

APPENDIX: DATA ACCESS STATEMENT

Data from the calculations including the optimized crystal structure, the calculated phonon and electronic dispersion and density-of-states (DoS), and the calculated dielectric function, are available free of charge from an online repository at https://doi.org/10.15125/BATH-00338.

[1] W. Albers, C. Haas, H. J. Vink, and J. D. Wasscher, J. Appl. Phys. **32**, 2220 (1961).
[2] H. Noguchi, A. Setiyadi, H. Tanamura, T. Nagatomo, and O. Omoto, Sol. Energy Mater. Sol. Cells **35**, 325 (1994).
[3] P. Sinsermsuksakul, L. Sun, S. W. Lee, H. H. Park, S. B. Kim, C. Yang, and R. G. Gordon, Adv. Energy Mater. **4**, 1400496 (2014).
[4] H. H. Park, R. Heasley, L. Sun, V. Steinmann, R. Jaramillo, K. Hartman, R. Chakraborty, P. Sinsermsuksakul, D. Chua, T. Buonassisi, and R. G. Gordon, Prog. Photovoltaics Res. Appl. **23**, 901 (2014).
[5] R. E. Banai, L. A. Burton, S. G. Choi, F. Hofherr, T. Sorgenfrei, A. Walsh, B. To, and J. R. S. Brownson, J. Appl. Phys. **116**, 13511 (2014).
[6] L. A. Burton and A. Walsh, Appl. Phys. Lett. **102**, 132111 (2013).
[7] V. Stevanović, K. Hartman, R. Jaramillo, S. Ramanathan, T. Buonassisi, and P. Graf, Appl. Phys. Lett. **104**, 211603 (2014).
[8] A. Rabkin, S. Samuha, R. E. Abutbul, V. Ezersky, L. Meshi, and Y. Golan, Nano Lett. **15**, 2174 (2015).
[9] A. N. Mariano and K. L. Chopra, Appl. Phys. Lett. **10**, 282 (1967).
[10] E. C. Greyson, J. E. Barton, and T. W. Odom, Small **2**, 368 (2006).
[11] D. Avellaneda, M. T. S. Nair, and P. K. Nair, J. Electrochem. Soc. **155**, D517 (2008).
[12] C. Gao, H. Shen, T. Wu, L. Zhang, and F. Jiang, J. Cryst. Growth **312**, 3009 (2010).
[13] I. Y. Ahmet, M. S. Hill, A. L. Johnson, and L. M. Peter, Chem. Mater. **27**, 7680 (2015).

[14] L. A. Burton and A. Walsh, J. Phys. Chem. C **116**, 24262 (2012).
[15] R. E. Abutbul, A. R. Garcia Angelmo, Z. Burshtein, M. T. S. Nair, P. K. Nair, and Y. Golan, CrystEngComm **18**, 5188 (2016).
[16] Rg.E. Abutbul, E. Segev, L. Zeiri, V. Ezersky, G. Makov, and Y. Golan, RSC Adv. **6**, 5848 (2016).
[17] P. K. Nair, A. R. Garcia-Angelmo, and M. T. S. Nair, Phys. Status Solidi Appl. Mater. Sci. **213**, 170 (2016).
[18] A. R. Garcia-Angelmo, R. Romano-Trujillo, J. Campos-Álvarez, O. Gomez-Daza, M. T. S. Nair, and P. K. Nair, Phys. Status Solidi **212**, 2332 (2015).
[19] A. Walsh and G. W. Watson, J. Phys. Chem. B **109**, 18868 (2005).
[20] J. M. Skelton, L. A. Burton, S. C. Parker, A. Walsh, C.-E. Kim, A. Soon, J. Buckeridge, A. A. Sokol, C. R. A. Catlow, A. Togo, and I. Tanaka, Phys. Rev. Lett. **117**, 75502 (2016).
[21] J. P. Perdew, A. Ruzsinszky, G. I. Csonka, O. A. Vydrov, G. E. Scuseria, L. A. Constantin, X. Zhou, and K. Burke, Phys. Rev. Lett. **100**, 136406 (2008).
[22] A. Walsh, D. J. Payne, R. G. Egdell, and G. W. Watson, Chem. Soc. Rev. **40**, 4455 (2011).
[23] K. M. Flood and D. L. Jaggard, J. Opt. Soc. Am. A **13**, 1395 (1996).
[24] J. Heyd, G. E. Scuseria, and M. Ernzerhof, J. Chem. Phys. **124**, 219906 (2006).
[25] J. Heyd and G. E. Scuseria, J. Chem. Phys. **121**, 1187 (2004).
[26] M. I. Aroyo, J. M. Perez-Mato, C. Capillas, E. Kroumova, S. Ivantchev, G. Madariaga, A. Kirov, and H. Wondratschek, Z. Kristallogr. - Cryst. Mater. **221**, 15 (2006).
[27] F. Brivio, K. T. Butler, A. Walsh, and M. van Schilfgaarde, Phys. Rev. B **89**, 155204 (2014).
[28] O. M. Madelung, *Semiconductors: Data Handbook,* 3rd ed. (Springer, Berlin, 2003).
[29] S. Bhattacharya, N. S. H. Gunda, R. Stern, S. Jacobs, R. Chmielowski, G. Dennler, and G. K. H. Madsen, Phys. Chem. Chem. Phys. **17**, 9161 (2015).
[30] C. Bera, S. Jacob, I. Opahle, N. S. H. Gunda, R. Chmielowski, G. Dennler, and G. K. H. Madsen, Phys. Chem. Chem. Phys. **16**, 19894 (2014).
[31] J. Vidal, S. Lany, M. d'Avezac, A. Zunger, A. Zakutayev, J. Francis, and J. Tate, Appl. Phys. Lett. **100**, 32104 (2012).
[32] Y. Kumagai, L. A. Burton, A. Walsh, and F. Oba, Phys. Rev. Appl. **6**, 14009 (2016).
[33] G. Kresse and J. Furthmüller, Phys. Rev. B **54**, 11169 (1996).
[34] G. Kresse and D. Joubert, Phys. Rev. B **59**, 1758 (1999).
[35] P. E. Blöchl, Phys. Rev. B **50**, 17953 (1994).
[36] A. Togo and I. Tanaka, Scr. Mater. **108**, 1 (2015).
[37] A. Togo, L. Chaput, and I. Tanaka, Phys. Rev. B **91**, 94306 (2015).
[38] A. A. Mostofi, J. R. Yates, G. Pizzi, Y.-S. Lee, I. Souza, D. Vanderbilt, and N. Marzari, Comput. Phys. Commun. **185**, 2309 (2014).
[39] A. A. Mostofi, J. R. Yates, Y. S. Lee, I. Souza, D. Vanderbilt, and N. Marzari, Comput. Phys. Commun. **178**, 685 (2008).
[40] M. Gajdos, K. Hummer, G. Kresse, J. Furthmüller, and F. Bechstedt, Phys. Rev. B **73**, 45112 (2006).